

2015

Drift of Plumes in the Mantle

Luke Douglas Brown
Portland State University

Follow this and additional works at: <https://pdxscholar.library.pdx.edu/honorstheses>

Let us know how access to this document benefits you.

Recommended Citation

Brown, Luke Douglas, "Drift of Plumes in the Mantle" (2015). *University Honors Theses*. Paper 201.
<https://doi.org/10.15760/honors.200>

This Thesis is brought to you for free and open access. It has been accepted for inclusion in University Honors Theses by an authorized administrator of PDXScholar. Please contact us if we can make this document more accessible: pdxscholar@pdx.edu.

DRIFT OF PLUMES IN THE MANTLE

by

Luke Douglas Brown

An undergraduate honors thesis submitted in partial fulfillment of the
requirements for the degree of

Bachelor of Science

in

University Honors

and

Geology

Thesis Advisor

Dr. Maxwell Lutman Rudolph

Portland State University

2015

DRIFT OF PLUMES IN THE MANTLE

Luke Douglas Brown
Advisor: Dr. Maxwell Lutman Rudolph

G 401 Project
An undergraduate thesis
submitted in partial fulfillment of the
requirements for the degree
Bachelor of Science
with Honors
at
Portland State University

2015

DRIFT OF PLUMES IN THE MANTLE

G 401

Presented by
Luke D. Brown

Abstract

We quantified the fixity of mantle plumes relative to the mantle in high Rayleigh number numerical thermal convection with radially- and temperature-dependent viscosity structures in a 3D spherical shell geometry. The relative velocities between plumes and the mantle increased with increasing Rayleigh number. Net migration rates of plumes vary from ~ 0.016 - $0.053^\circ/\text{Myr}$, and differential plume velocities can be up to $\sim 25\%$ of past- and present-day rates of net lithospheric rotation. Individual plumes migrate on average at ~ 0.0617 - $0.223^\circ/\text{Myr}$ for Rayleigh numbers between $1 \cdot 10^7$ and $2 \cdot 10^8$. We compared the ratio of plume velocity to horizontal average velocity (a) at the surface and (b) at mid-mantle for experiments with Rayleigh number between $5 \cdot 10^7$ and $2 \cdot 10^8$, which were (a) ~ 0.15 and (b) ~ 0.35 . Additionally, we plotted the mean migration rates of plumes against Rayleigh number and found that a linear fit had a greater R^2 value than a power law fit. There is a transition in the long-wavelength structure of convection from degree-2 to degree-1 poloidally dominant motion between $Ra = 1 \cdot 10^7$ and $Ra = 2 \cdot 10^7$ where thermal upwellings change from dominantly sheet-like to dominantly plume-like. Future studies should investigate whether the scaling of plume velocities with vigor of convection depends on the mode of convection. We find that all cases produce long-lived plume-like features which generate from a thermal boundary layer at the core-mantle boundary, and persist for more than 80 Myr. On average, the lifespan of mantle plumes decreased with increasing Rayleigh number. Our studies suggest that hotspots may be an imperfect proxy for a lower mantle reference frame.

Advisor

Dr. Maxwell L. Rudolph

Department Chair

Dr. Martin J. Streck

Portland State University
2015

1 Introduction

Some intraplate volcanism, associated with hotspots, may be surface manifestations of thermal upwellings in the mantle, which *Morgan* (1971) suggested were sourced from the lower mantle. He referred to these upwellings as ‘plumes’. Thermal plumes are thin, quasi-cylindrical conduits of hot mantle material and are a basic form of heat transport by thermal convection in the mantle. When they impinge upon the lithosphere, plume heads can produce massive outpourings of basaltic lava, as suggested for the Deccan Traps. Afterward, long-lived plume tails continue to supply hot material to the surface and are recorded as hotspot tracks. For example, the hotspot track associated to the Deccan Traps is Réunion. The origin of thermal plumes has remained inconclusive because of a lack of direct evidence. Seismic tomographic data currently fails to resolve plume tails at depth. A slow shear-wave velocity anomaly should correlate with the anomalously hot mantle plume tail. Accordingly, alternative models for the origin of hotspot volcanism have suggested an asthenospheric or other mechanism [*Anderson and King*, 2014]. However, *Courtillot et al.* (2003) have collected various lines of evidence to support the existence of multiple possible sources of thermal plumes in the mantle. These include geochemical contrasts of $^3\text{He}/^4\text{He}$ and $^{21}\text{Ne}/^{22}\text{Ne}$ ratios between mid-ocean ridge basalts (MORBs) and ocean island basalts (OIBs), correlation of Large Igneous Provinces (LIPs) with impinging mantle plume heads, laboratory studies of thermal convection in viscous fluids [*Whitehead and Luther*, 1975; *Jellinek and Manga*, 2004], numerical convection studies [*Steinberger and O’Connell*, 1998; *Zhong et al.*, 2000, *Zhong et al.*, 2001; *McNamara and Zhong*, 2004; *Zhong et al.*, 2008], and seismic imaging of the deep mantle beneath Hawaii and Iceland [*Wolfe et al.*, 1997]. *Sleep* (2006) has also investigated the origins of plumes using first principles and found that thermal boundary layers at the core-mantle boundary and 410-670 km transition zone result in thermal instabilities which generate thermal upwellings. In high Rayleigh number thermal convection, the thermal boundary layers generate plumes repeatedly [*Schubert and Turcotte*, 2001].

Hotspots are often associated with nearly linear chains of volcanic edifices such as the Hawaiian-Emperor Seamount track. *Morgan* (1971) argued that hotspot tracks record the history of plate motions. He and others estimated that hotspots remained relatively fixed compared to plate migration rates, as well as fixed relative to each other [*Duncan*, 1981; *Morgan*, 1983]. However, it was discovered that there is relative motion (1 to 2 cm per year) between hotspots under the Pacific and Indo-Atlantic plates, so that a global

fixed hotspot reference frame is not accurate [Molnar and Stock, 1987]. Thus, moving hotspot reference frames were introduced to define absolute frames of reference for quantifying various global processes such as lithospheric plate motions, net lithospheric rotation, and true polar wander [Rudolph and Zhong, 2014; Doubrovine *et al.*, 2012; Conrad and Behn, 2010]. The definition of moving hotspot reference frames is based on the assumption that mantle plumes, and their hotspots, are representative of a stable lower mantle [Doubrovine *et al.*, 2012; Seton *et al.*, 2012]. Numerical models of mantle plume migration provide a window into the differential motion between mantle plume conduits and the ambient mantle that is relatively intractable for laboratory experiments of thermal convection in viscous fluids. McNamara *et al.* (2004) have investigated the relative fixity of plume conduits against the lower mantle under purely thermal and thermochemical convection in a Cartesian domain with depth- and temperature-dependent viscosity structures. They find that a chemically dense layer present in thermal convection has negligible effect upon the relative fixity of mantle plumes compared to purely thermal convection with no-slip and free-slip boundary conditions.

We tested the hypothesis that mantle plumes are fixed relative to the ambient mantle flow in a spherical shell geometry using the finite element code CitcomS. CitcomS is a community code that can be used to solve three-dimensional numerical simulations of high Rayleigh number thermal convection in a spherical shell geometry. We studied the effects of temperature- and radially-dependent viscosity structures, as well as different Rayleigh numbers, on mantle plume presence and lateral migration rates relative to a lower mantle reference frame.

The rest is organized as follows: in Section 2, we will describe the governing equations and nondimensionalisation of input parameters, define parametrizations of Rayleigh number and viscosity structure, and describe initial and boundary conditions, the CitcomS mesh, and quantification of numerical output. In Section 3, we present calculated plume persistence and net lateral plume migration rates relative to an absolute lower mantle reference frame. In Sections 4 and 5, we discuss our results and state conclusions.

2 Methods

2.1 Governing Equations

Thermal convection in a three-dimensional spherical shell geometry is governed by the equations of mass, momentum, and energy. The mantle is treated as an anelastic, incompressible, viscous spherical shell where incompressibility follows from the Boussinesq approximation. With these assumptions, the governing equations are:

$$\nabla \cdot \underline{u} = 0 \quad (1)$$

$$-\nabla p + \nabla \cdot [(\eta(\nabla \underline{u} + \nabla^T \underline{u}))] - \delta \rho g_0 \hat{e}_r = 0 \quad (2)$$

$$\rho C_p \left(\frac{\partial T}{\partial t} + \underline{u} \cdot \nabla T \right) = k \nabla^2 T + \rho_0 H \quad (3)$$

where \underline{u} is the velocity in a nonrotating mantle reference frame; p is the dynamic pressure; η_0 , ρ_0 , k , and C_p are mantle reference viscosity, density, thermal conductivity and specific heat capacity, respectively; g_0 , T , and H are acceleration due to gravity, temperature, and internal heat source, respectively; t is the time; and \hat{e}_r is the unit vector in the radial direction. The object $\delta \rho$ in equation (2) represents density perturbations. Only thermal expansion contributes to density perturbations, i.e. we ignore compositional heterogeneities; therefore, $\delta \rho$ can be expressed by

$$\delta \rho = -\rho_0 \alpha (T - T_0) \quad (4)$$

where α is the thermal expansivity and T_0 is a reference temperature taken to be the temperature at mid-mantle.

The governing equations may be nondimensionalized as in the work of *Zhong et al.* (2000) and *Zhong*

et al. (2008) via:

$$\begin{aligned}
r &= R_0 r' \\
t &= \frac{R_0^2}{\kappa} t' \\
\rho &= \rho_0 \rho' \\
\mathbf{u} &= \frac{\kappa}{R_0} \mathbf{u}' \\
T &= \Delta T T' + T_0 \\
\eta &= \eta_0 \eta' \\
P &= \frac{\eta_0 \kappa}{R_0^2} P'
\end{aligned} \tag{5}$$

where R_0 is the planetary radius, $\kappa = \frac{k}{\rho_0 C_p}$ is the thermal diffusivity, and ΔT is the temperature drop between the core-mantle boundary (CMB) and the surface. All model calculations are in a spherical shell geometry, and the above rescaling yields $r_b = 0.55$ at the CMB and $r_o = 1$ at the surface. Other physical parameters are constant besides viscosity, which is parametrized below. The values of other parameters are summarized in Table 1.

Substituting equations (4) and (5) into equations (1)-(3) and dropping the primes, the nondimensionalized governing equations are:

$$\nabla \cdot \mathbf{u} = 0, \tag{6}$$

$$-\nabla P + \nabla \cdot [(\eta(\nabla \mathbf{u} + \nabla^T \mathbf{u}))] + Ra T \hat{\mathbf{e}}_r = 0, \tag{7}$$

$$\frac{\partial T}{\partial t} + \mathbf{u} \cdot \nabla T = \nabla^2 T + \gamma \tag{8}$$

where Ra is a thermal Rayleigh number measuring the vigor of convection, and γ is the nondimensional internal heating rate. The expressions for Ra and γ are

$$\begin{aligned}
Ra &= \frac{\rho_0 \alpha \Delta T g_0 R_0^3}{\kappa \eta_0}, \\
\gamma &= \frac{R_0^2}{\kappa C_p \Delta T} H
\end{aligned} \tag{9}$$

Parameter	Value	Units
R_0	6.371×10^6	m
g_0	9.8	m s^{-2}
ρ_0	3000	kg m^{-3}
C_p	1250	$\text{J kg}^{-1} \text{K}^{-1}$
α	3×10^{-5}	K^{-1}
κ	1×10^{-6}	$\text{m}^2 \text{s}^{-1}$
k	3.75	$\text{Wm}^{-1} \text{K}^{-1}$
ΔT	2500	K

Table 1: Summary of constant and reference model parameters for the experiments

CitcomS uses the radius of Earth instead of mantle layer thickness to parametrize the thermal Rayleigh number. Our calculations omitted radiogenic heating, so that $H = \gamma = 0$.

2.2 Boundary Conditions and Initial Values

We imposed free-slip boundary conditions at the surface and bottom boundaries to simulate the stress conditions between the upper mantle and atmosphere as well as between the lower mantle and liquid outer core. We also imposed isothermal boundary conditions with nondimensional temperatures of 0 and 1 at the top and bottom boundaries, respectively.

The initial condition is a statement about the initial temperature field: it is a conductive profile with uniform temperature $T_m = 0.5$ everywhere in the domain except for a cold thermal boundary layer along the top boundary and a warm thermal boundary layer along the bottom boundary. The initial temperature profile is expressed by

$$T(r, \theta, \phi) = \delta \sin\left(\frac{(r - r_b)\pi}{(r_o - r_b)}\right) \cdot (\sin(m\phi) + \cos(m\phi)) P_{lm}(\cos(\theta)) \quad (10)$$

where $\delta = 0.01$ is the magnitude of perturbation given to all layers; l and m are spherical harmonic degree and order; r , θ , and ϕ are the radial, longitudinal and colatitudinal coordinates; and P_{lm} is the associated Legendre polynomial

$$P_{lm}(x) = \frac{(-1)^m}{2^l l!} (1 - x^2)^{\frac{m}{2}} \frac{d^{l+m}}{dx^{l+m}} (x^2 - 1)^l \quad (11)$$

which was normalized such that the spherical harmonic basis functions are expressed by

$$Y_{lm}(\theta, \phi) = \begin{cases} \sqrt{2} \sqrt{\frac{(2l+1)}{4\pi} \frac{(l-|m|)!}{(l+|m|)!}} P_{lm}(\cos(\theta)) \cos(|m|\phi) & \text{if } m < 0, \\ \sqrt{\frac{(2l+1)}{4\pi} \frac{(l-m)!}{(l+m)!}} P_{lm}(\cos(\theta)) & \text{if } m = 0, \\ \sqrt{2} \sqrt{\frac{(2l+1)}{4\pi} \frac{(l-m)!}{(l+m)!}} P_{lm}(\cos(\theta)) \cos(m\phi) & \text{if } m > 0 \end{cases} \quad (12)$$

2.3 Model Descriptions

We conducted numerical experiments of thermal convection in an Earth-like mantle to quantify the migration rates of thermal plumes at depth. Starting from a basic case of isoviscous rheology, we introduced more complexity to control for the behavior of each change in parameter space. The model cases test the effects of constant, depth-dependent, and temperature-dependent viscosity, as well as effects of different Rayleigh numbers. The rheology law defining the temperature-dependent viscosity for all cases is given by the expression

$$\eta = \eta_0 \exp(E_\eta(T_\eta - T)) \quad (13)$$

where $E_\eta = 9.2102404$ is equivalent to the activation energy and comes from prescribing a 10^4 viscosity contrast between the CMB and the surface; $T_\eta = 0.5$ is the initial temperature at mid-mantle depth; and η_0 is a depth-dependent viscosity pre-factor.

We now describe the six cases tested in the experiment. The first (case 1) is a base case with an isoviscous rheology. Case 2 is identical to case 1 but includes a temperature-dependent viscosity as in (13). We introduced a layered viscosity structure, i.e. a depth-dependent viscosity, to cases 3, 4, 5 and 7 in addition to the temperature-dependent viscosity defined for case 2. The layers correspond to a highly viscous lithosphere with bottom boundary at ~ 150 km depth, a weak transition zone, and a lower mantle. Representative viscosity profiles with depth are shown in Figure 1.

Cases 3, 4, 5 and 7 vary in Rayleigh number, Ra , as in (9). Prescribing the Rayleigh number also defines η_0 , or the value for the reference viscosity. The depth dependent viscosities are relative to η_0 , which decreased 30-fold at 150 km depth and increased 20-fold at 670 km relative to the 150 km to 670 km weak zone. Cases 3, 4, 5 and 7 are otherwise identical. Table 2 summarizes the parameters for each experiment.

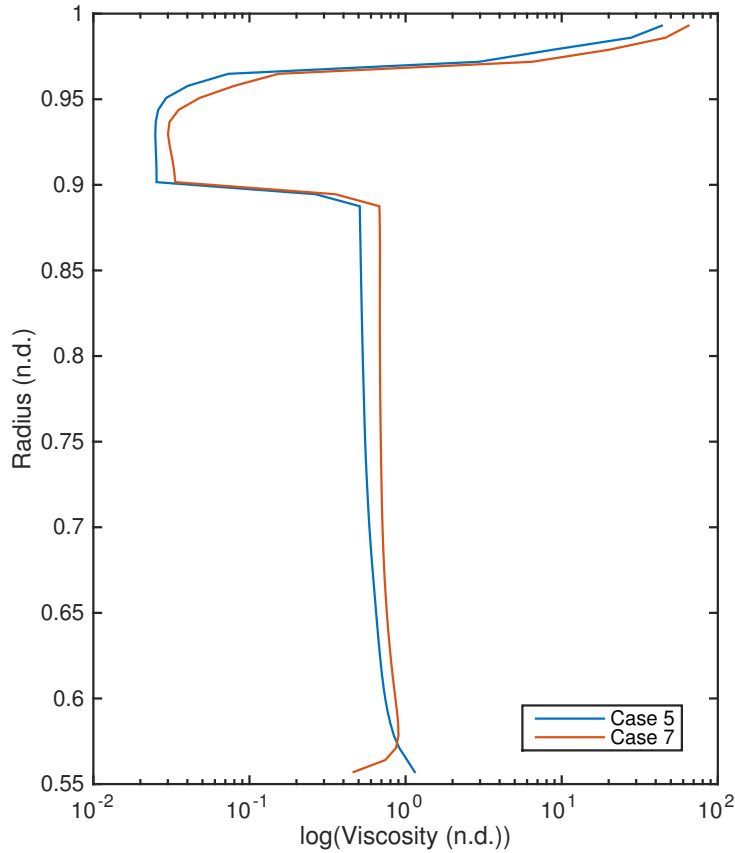


Figure 1: *Representative viscosity profile with depth.* Nondimensional, horizontally averaged viscosity contrasts defined for the (a) lithosphere is 0.0235479, (b) weak zone is 0.06435 (410 km) and 0.10519 (670 km), and (c) core-mantle boundary is 0.45. There is a 30-fold decrease in viscosity in the weak zone, followed by a 20-fold increase in viscosity of the lower mantle relative to the weak zone.

2.4 CitcomS

The equations of mass, momentum, and energy were solved using CitcomS [Zhong *et al.*, 2001]. The mesh resolution was $12 \times (64 \times 64 \times 64)$ for every case; CitcomS partitions the spherical shell into 12 caps, each with 64 brick elements in the radial, longitudinal, and colatitudinal directions. This provides horizontal resolution at the outer surface of approximately 1 degree. We chose this resolution because the diameters of mantle plumes are estimated to be on the order of 100 km; hence, this numerical resolution is fine enough to detect plumes.

Case Number	Rayleigh Number (Ra)	Reference Viscosity η_0 (Pa·s)	Temperature Dependence	Depth Dependence
1	1.0×10^8	5.70×10^{21}	No	No
2	1.0×10^8	5.70×10^{21}	10^4	No
3	1.0×10^8	5.70×10^{21}	10^4	Yes
4	5.0×10^7	1.14×10^{22}	10^4	Yes
5	2.0×10^8	2.85×10^{21}	10^4	Yes
7	1.0×10^7	5.70×10^{22}	10^4	Yes

Table 2: Summary of parameters that vary between different cases discussed in text.

2.5 Plume Tracking

We ran each calculation to statistically steady state in terms of average heat flow, mean internal temperature, and RMS velocity. We then restarted each calculation and saved temperature and velocity output at high temporal frequency for plume tracking. Starting from the 3D spherical geometry output, we identified plumes at mid-mantle depth as anomalies 24% warmer (nondimensional temperature anomaly $T' = 0.12$, dimensional temperature anomaly $T = 300$ K) than horizontal average at this depth; the calculated plume presence and lateral migration rates were insensitive to variations in the warm anomaly threshold. We tracked plumes between timesteps by matching each plume at timestep (n+1) with the most similar feature at timestep (n). If no similar feature existed, we accounted for the creation of a new plume. Destruction of plumes is handled by default in our algorithm when some plumes are simply not identified at timestep (n+1). We defined a lower mantle reference frame to measure lateral migration rates using mantle net rotation calculations obtained via CitcomS, and the expressions in *Zhong* (2001, Appendix A).

3 Results

We now present quantified data from the CitcomS output. Our calculations are for thermal convection at statistical steady-state in terms of horizontally averaged quantities, namely horizontal and vertical RMS velocity components and temperature. Degree-1 poloidal motion of plumes is evident in cases 3, 4 and 5; the global motion of plumes (positive thermal anomalies) is convergence at a pole that is nearly antipodal to where cold downwellings converge. In cases 3 and 4, plumes migrate toward the south pole, while in case 5, the dominant direction of plume migration is north. This difference is superfluous; rotational forces are not

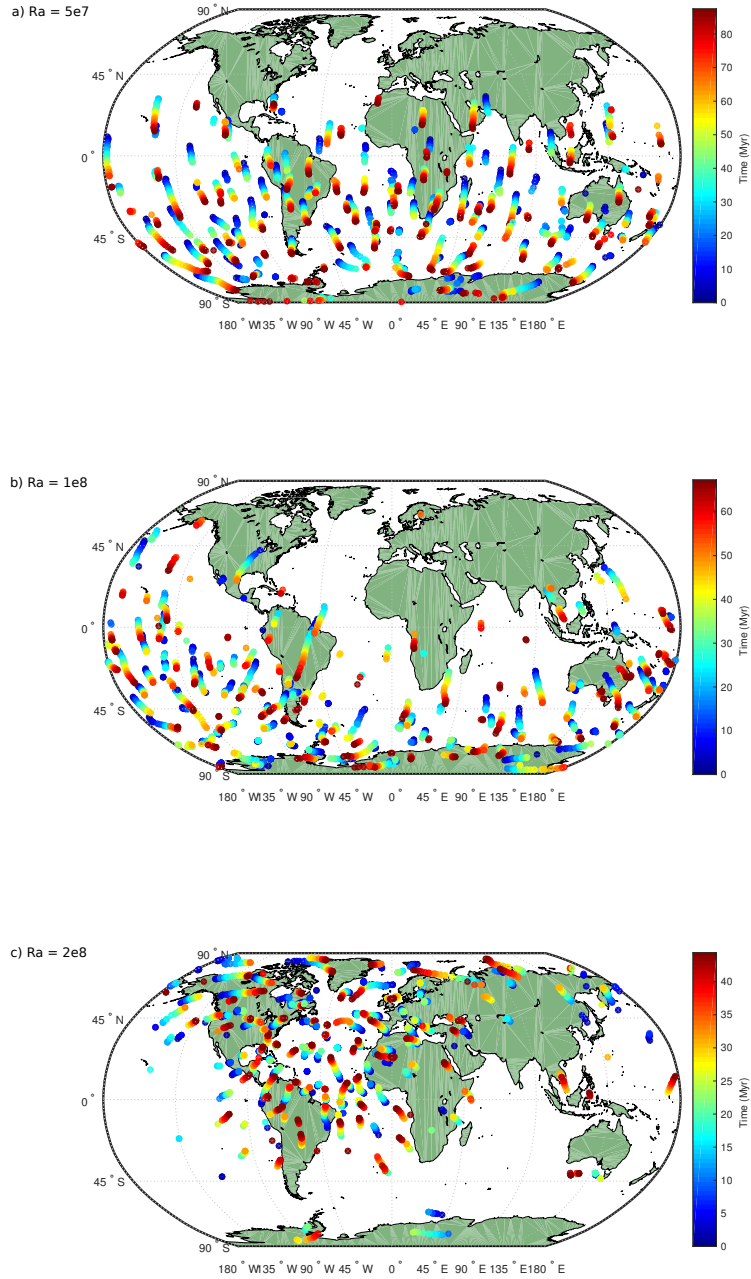


Figure 2: *Plume Tracks*. Circle markers denote the locations of thermal anomalies at each timestep, and plume conduits leave tracks of their lateral migration over time. The tracks in the figure move laterally inside a spherical shell at mid-mantle depth, and the world map is displayed to give perspective of motion on the sphere. Degree-1 toroidal motion is dominant in all cases, where the hot thermal anomalies converge to a location antipodal to the location of cold thermal anomaly convergence. The average lifetime of plumes in (a) is 38 Myr, (b) is 26.7 Myr, and (c) is 13.6 Myr. The different times elapsed are (a) 90 Myr, (b) 70 Myr, and (c) 50 Myr.

thought to play a significant role in mantle dynamics, and because we chose free-slip boundary conditions, the choice of reference frame is arbitrary. Case 7 exhibits a different regime of parameter space than the other cases. Thermal upwellings in case 7 (associated with a positive thermal anomaly with nondimensional temperature greater than $T' = 0.12$) are predominantly sheet-like, with occasional diapiric structures. Figure 3 gives a visualization of the degree-2 and degree-1 poloidal convection styles of case 7 and case 5.

We determined the amount of time that hot thermal anomalies remained active. A significant number of hot thermal anomalies detected by our algorithm were present for a single output step (or approximately 3.1, 2.3, 1.6, or 1.1 Myr in cases 7, 4, 3 and 5, respectively). We found that 19.7%, 19.3%, 17.7% and 15.6% of hot anomalies were transient in cases 7, 4, 3, and 5, and differentiated these from plume-like features. The life expectancy of plumes in thermal convection with both temperature- and depth-dependent viscosity decreased with increasing Rayleigh number. When we omitted the contribution to mean life expectancy by transients, the average plume in case 7 ($Ra = 1 \cdot 10^7$) persisted for 66 Myr with standard deviation 129.7 Myr, persisted for 38 Myr with a standard deviation of 48.2 Myr in case 4 ($Ra = 5 \cdot 10^7$), for 21.7 Myr with standard deviation 26.7 Myr in case 3 ($Ra = 1 \cdot 10^8$), and 13.6 Myr with standard deviation 16.2 Myr in case 5 ($Ra = 2 \cdot 10^8$). We report the standard deviation for each case as a measure of the spread of plume lifetimes, but also acknowledge that the distribution of plume lifetimes may not be normal. Figure 4 shows that the distribution of plume lifetimes is skewed toward short lifespans. The average number of plumes at any given instant in time (in Myr) was 24, 73, 62, and 54, for cases 7, 4, 3, and 5, respectively.

We computed the lateral velocities of plume conduits in a lower mantle reference frame defined by the method outlined by *Zhong* (2001, Appendix A). The average plume speed of individual plume conduits (Figure 5) and average net plume migration rates (Figure 6) in temperature- and depth-dependent viscosity thermal convection increased with increasing Rayleigh number. The average plume speed refers to the total displacement of plume conduits over their lifespan. The average plume speed for cases 7, 4, 3, and 5 was $0.0617^\circ/\text{Myr}$, $0.1714^\circ/\text{Myr}$, $0.211^\circ/\text{Myr}$, and $0.233^\circ/\text{Myr}$, respectively. The calculated differential velocities between the net migration rate of plumes and the lower mantle net rotation rate varied in time (Figure 5). The average net migration rates of plumes were $0.01615^\circ/\text{Myr}$, $0.0214^\circ/\text{Myr}$, $0.0326^\circ/\text{Myr}$, and $0.0534^\circ/\text{Myr}$, for cases 7, 4, 3, and 5, respectively.

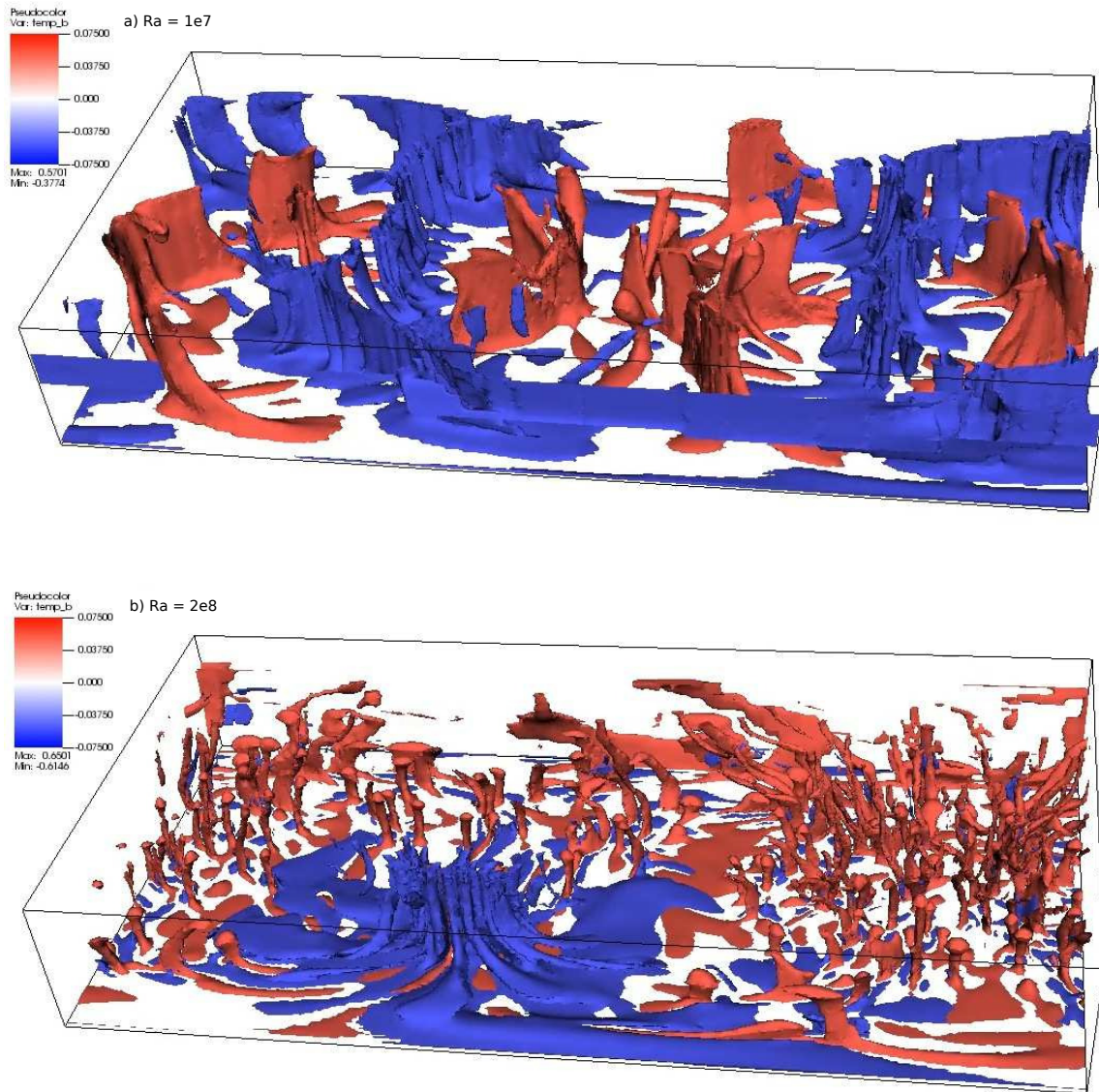


Figure 3: *Cases 7 and 5 at Statistically Steady-State Thermal Convection.* Freeze-frame of residual temperature isosurfaces of thermal convection for modes of convection at statistically steady-state dominated by (a) degree-2 poloidal motion and (b) degree-1 poloidal motion. Thermal upwellings (red) and downwellings (blue) are shown with nondimensional temperature variation $T' \leq |0.075|$. Thermal upwellings in (a) are dominantly sheet-like with some thermal plumes. Thermal upwellings in (b) are dominantly plume-like.

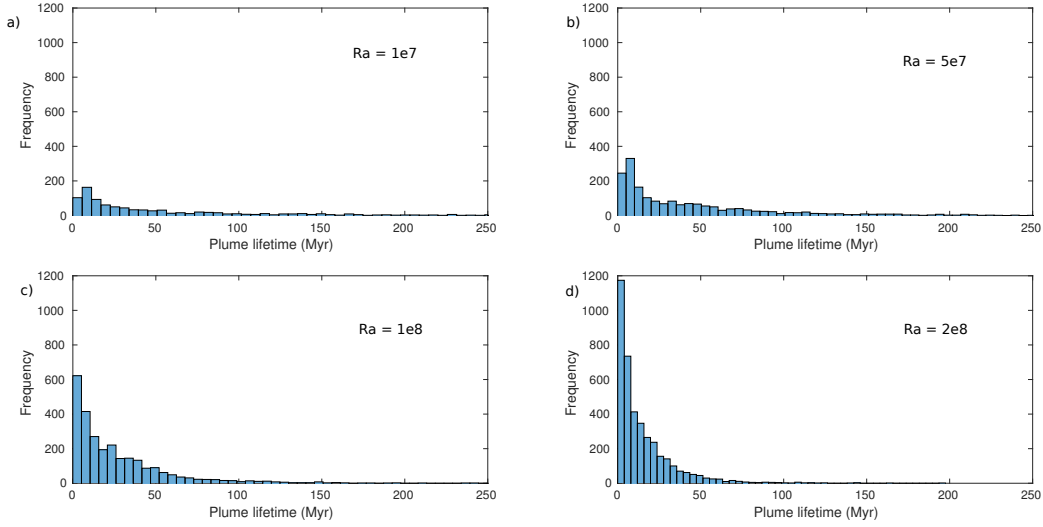


Figure 4: *Life expectancy of plumes*. Distribution of plume lifespans in Myr. The time elapsed for calculating plume lifetimes was fixed to 900 Myr. These histograms omit the contribution of short-lived transients. The lifespan of omitted positive thermal anomalies in each case was less than (a) 3.1 Myr, (b) 2.3 Myr, (c) 1.6 Myr, and (d) 1.1 Myr. Multiple hot thermal anomalies are long-lived features, and are present in all cases.

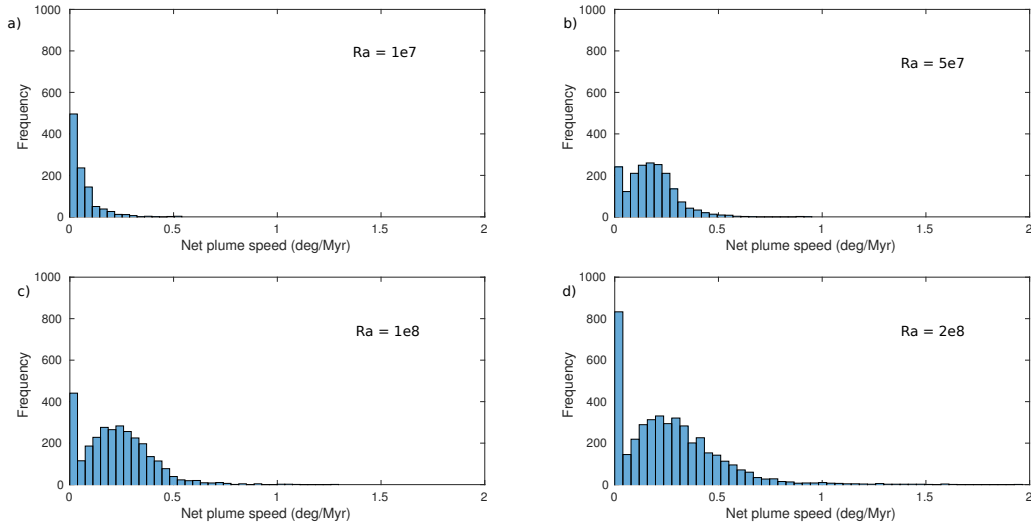


Figure 5: *Frequency distribution of mean plume speeds in a lower mantle reference frame*. Time elapsed for all cases in this calculation is 900 Myr. The mean plume speed in (a) is $0.0617^\circ/\text{Myr}$, (b) is $0.1714^\circ/\text{Myr}$, (c) is $0.211^\circ/\text{Myr}$, and (d) is $0.233^\circ/\text{Myr}$. There are fewer plumes in (a) than other cases because the mode of convection was degree-2 poloidal (in contrast to degree-1 poloidal in cases 3, 4, and 5), where thermal upwellings and downwellings are dominantly sheet-like. Cold downwellings tend to control the motion of hot anomalies, and the symmetry of convection in (a) stabilized the diapiric structures [McNamara and Zhong, 2004]. These results do not omit transients, but transient features necessarily have zero speed.

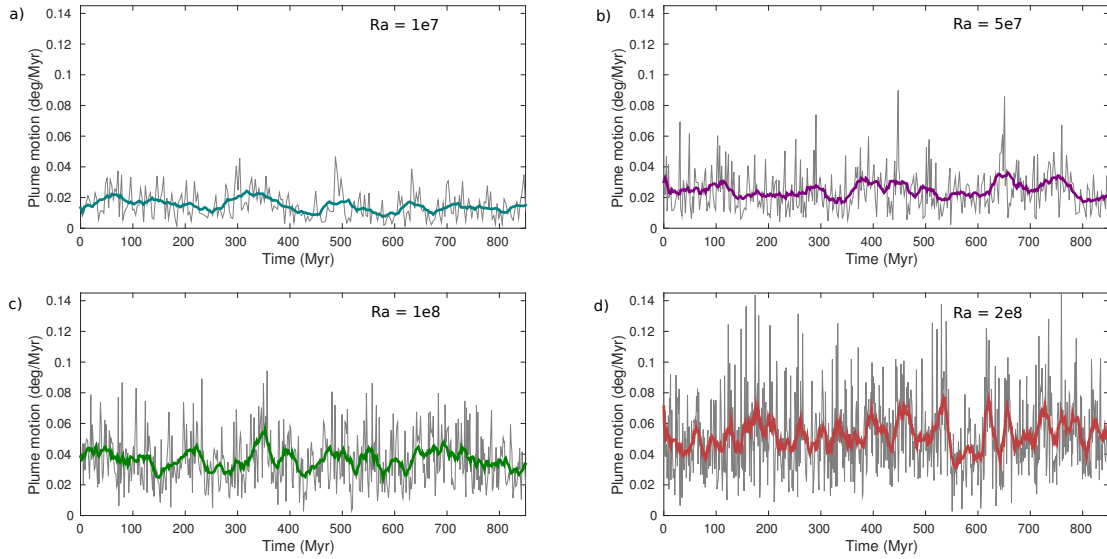


Figure 6: *Net migration rates of plumes in a lower mantle reference frame.* The light grey curve in each panel is the raw net migration rate of plumes at each timestep, and the colored curve is a smoothed version. The average net migration rate of mantle plume conduits increases with increasing Rayleigh number. The mean net migration rate in (a) is $0.01615^{\circ}/\text{Myr}$, (b) is $0.0214^{\circ}/\text{Myr}$, (c) is $0.0326^{\circ}/\text{Myr}$, and (d) is $0.0534^{\circ}/\text{Myr}$. The net migration rate can be thought of as the lateral velocity of the average plume.

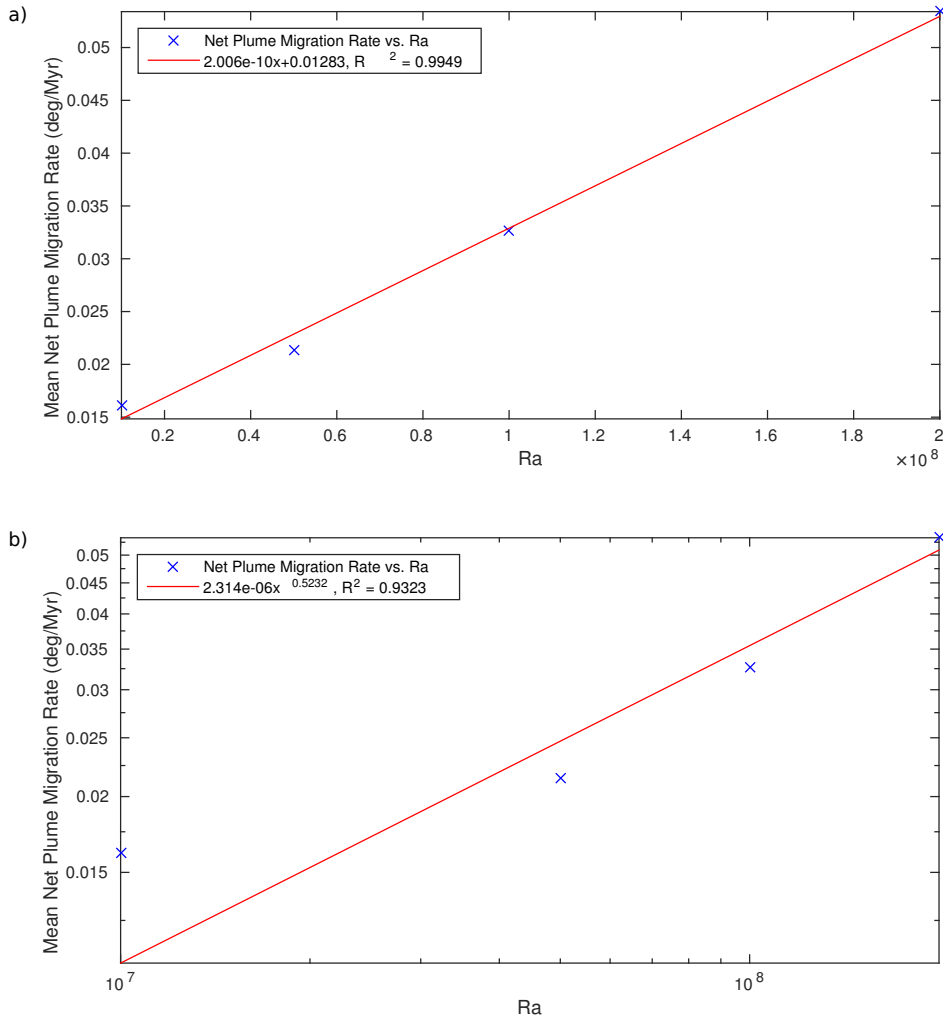


Figure 7: *Scaling relationship of mean net plume migration rate with Rayleigh number.* Data points (blue x's) are the mean net plume migration rate in $^{\circ}/\text{Myr}$ plotted against Rayleigh number. The mean net migration rate of plumes increases with increasing Rayleigh number. We provide two best-fitting curves assuming (a) a linear relationship with 95% confidence bounds and (b) a power law relationship with 95% confidence bounds. Error bounds for coefficients in (a) are $(1.57 \cdot 10^{-10}, 2.442 \cdot 10^{-10})$ and $(0.007836, 0.01783)$. Error bounds for the coefficient and exponent in (b) are $(-2.032 \cdot 10^{-5}, 2.495 \cdot 10^{-5})$ and $(-0.0005153, 1.047)$.

4 Discussion

Global moving hotspot reference frames approximate that mantle plume conduits remain fixed relative to mantle flow, in the sense that the global net migration rate of hotspots is representative of a “mean mantle” [Dobrovine *et al.*, 2012]. The net rotation of the lithosphere (hereafter referred to by NLR) is closely

related to this assumption because an absolute frame of reference is required to distinguish between rigid rotations of the lithosphere and mantle together (true polar wander) and differential rotation between the lithosphere and mantle [Rudolph and Zhong, 2014]. Present-day net rate of lithospheric rotation (NRLR) is estimated between $0.11^\circ/\text{Myr}$ and $0.44^\circ/\text{Myr}$ with uncertainties of $\sim 25\%$ or greater. It is estimated that NRLR was greater in the past, with rotation rates up to $\sim 0.7^\circ/\text{Myr}$ [Seton *et al.*, 2012; Rudolph and Zhong, 2014; Doubrovine *et al.*, 2012]. These geodynamic models measure NLR and NRLR under moving hotspot reference frames. Conrad and Behn (2010) suggest an upper bound of $<0.26^\circ/\text{Myr}$ NRLR using SKS splitting observations for an asthenosphere 10 times less viscous than the upper mantle; they include that the upper bound decreases with larger viscosity contrasts between lithospheric mantle and asthenosphere. Becker (2008) constrained NLR by studying azimuthal anisotropy in the mantle induced by net rotation of the lithosphere and estimated that NRLR can only be $\sim 1/2$ ($\sim 0.22^\circ/\text{Myr}$) of NLR predicted by the hotspot reference frame HS3 [Gripp and Gordon, 2002].

Our models examined the relationship of mid-mantle plume fixity and convective vigor in a mantle with free-slip boundary conditions at the surface and CMB and temperature- and depth-dependent viscosity structure. We note that the behavior of dynamical systems is determined by boundary and initial conditions, and we acknowledge the possible differences between free-slip boundary conditions and prescribed time-dependent plate velocity boundary conditions on the lateral migration rates of plume conduits in Earth's mantle [Zhong *et al.*, 2000]. From our simulations we calculated differential rates of motion between the lower mantle and thermal anomalies at mid-mantle depth on the order of hundredths of degrees per Myr.

We can use the net rates of migration of plumes corresponding to different Rayleigh numbers to compare lateral migration rates of plume conduits to average plate velocities at the surface. Gripp and Gordon (2002) provide estimates for fast-moving plates at $\sim 1^\circ/\text{Myr}$ (e.g. the Pacific plate), the median plate velocity at $\sim 0.3^\circ/\text{Myr}$ (e.g. Nazcan and North American plates), and slow-moving plates at $\sim 0.1-0.2^\circ/\text{Myr}$ (e.g. African plate). The lateral velocity ratio between our plumes and these plate velocity estimates are as follows: for fast-moving plates, the range is 0.016-0.053; for the median plate speed the range is 0.054-0.178; for slow-moving plates, the range is 0.108-0.356. The average net migration of plumes over the period of a plume lifetime such as the plume beneath the Hawaiian-Emperor seamount chain (~ 80 Myr) is bounded above by 76 km. Compared to the lateral extent traced by lithospheric plates such as the African plate, the

ratio of plume migration to plate motion is at most ~ 0.17 between the net migration of plumes and slowest plates.

McNamara and Zhong (2004) tested the relative fixity of mantle plumes in thermal and thermochemical convection in a Cartesian domain with Rayleigh numbers $5 \cdot 10^6$ and $1 \cdot 10^7$. They quantified plume fixity using a ratio of horizontal plume velocity to horizontal average velocity at the top boundary, to which we compare our own lateral velocity ratio (LVR, an acronym which we will use for their results and ours). Note that our Rayleigh number was parametrized by the radius of Earth, whereas *McNamara and Zhong* (2004) defined their Rayleigh number by mantle layer thickness. This difference results in an approximately 11 fold difference in Rayleigh number for thermal convection with equivalent vigor. Since the Rayleigh numbers of our four cases are on the order of $\sim 1 \cdot 10^7$ and $\sim 1 \cdot 10^8$, the vigor of convection for each of our studies is directly comparable to theirs. Their thermochemical cases found similar LVR to the isochemical cases with no-slip boundary conditions, where LVR ranged from ~ 0.37 to 0.47 for $Ra = 5 \cdot 10^6$ and from ~ 0.32 to 0.5 for $Ra = 1 \cdot 10^7$. The plumes in isochemical cases with free-slip boundary conditions were more stable, with LVR between ~ 0.17 and 0.37 for $Ra = 5 \cdot 10^6$ and between ~ 0.21 and 0.34 for $Ra = 1 \cdot 10^7$ [*McNamara and Zhong*, 2004]. We found that for our four cases the LVR between thermal plumes and the surface were 1.06 ($Ra = 1 \cdot 10^7$), 0.16 ($Ra = 5 \cdot 10^7$), 0.15 ($Ra = 1 \cdot 10^8$), and 0.15 ($Ra = 2 \cdot 10^8$). The LVR between plumes in each case and the mid-mantle was 1.23 ($Ra = 1 \cdot 10^7$), 0.36 ($Ra = 5 \cdot 10^7$), 0.34 ($Ra = 1 \cdot 10^8$), and 0.35 ($Ra = 2 \cdot 10^8$). Case 7 ($Ra = 1 \cdot 10^7$) has significantly larger LVR than the other cases. An LVR greater than 1 implies that hot anomalies are migrating laterally at a faster rate than both the average velocity at the surface and at mid-mantle depth. As observed in Figure 3, the style of convection is distinct between cases 7 and the others. Due to its lower Rayleigh number, case 7 may exhibit ‘stagnant-lid’ convection, which would account for the faster velocities of hot anomalies at depth compared to the surface. The similar LVR between cases 3-5 shows that relative to the ambient mantle flow, the differential velocities of plumes in the mantle scale with Rayleigh number. Figure 7a shows this relationship from another perspective, where the mean net migration rate of plumes increases with increasing Rayleigh number. We provide two goodness-of-fit lines defined by (7a) a linear equation and (7b) a power law equation. The R^2 value for the linear fit is greater than for the power law.

The flow pattern for mantle plume conduits is dominated by degree-1 poloidal motion in cases 3, 4, and 5

with Rayleigh number $5 \cdot 10^7$ or greater. Case 7 ($Ra = 1 \cdot 10^7$) exhibited degree-2 poloidal motion, which has a different mantle thermal structure with predominantly sheet-like thermal upwellings surrounded by sheet-like downwellings. We compared cases 7 and 5 visually in Figure 3. *McNamara and Zhong* (2004) used a nondimensional thermal anomaly of +0.1 for their mantle plumes, and our calculations considered thermal anomalies at +0.12 (n.d.) above mean mantle temperature. Our calculated results were unaffected by selecting this temperature threshold. Cold thermal downwellings attenuate the drift of hot thermal anomalies in the mantle flow in degree-2 dominated convection; in the degree-1 dominated cases, the cold downwellings can increase the drift of hot anomalies relative to the mantle [*McNamara and Zhong*, 2004].

5 Conclusions

We quantified the differential velocity between plumes and the mantle in high Rayleigh number thermal convection. The net migration rates of plumes vary from ~ 0.02 - $0.053^\circ/\text{Myr}$, and differential plume velocities can be up to $\sim 25\%$ of past- and present-day rates of net lithospheric rotation. This suggests that the validity of assuming that the motions of hotspots are representative of the mantle should be further investigated.

There is a transition of convective style between $Ra = 1 \cdot 10^7$ and $Ra = 5 \cdot 10^7$, which we showed in Figure 3. Temperature- and radial-dependence of viscosity sufficed to produce long-wavelength thermal structures in the mantle, similar to [*Zhong et al.*, 2000]. The long-wavelength structure in case 7 ($Ra = 1 \cdot 10^7$) is degree-2 poloidal and in cases 3-5 is degree-1 poloidal. The structure of thermal upwellings changed from dominantly sheet-like to dominantly plume-like through the transition. Case 7 may exhibit stagnant lid convection in which a relatively thick, cold, rigid thermal boundary layer forms at the top boundary. This mode of convection is observed in some planetary bodies.

We found that the life expectancy of plumes decreased with increasing vigor of convection. In all cases, there were plumes that were long-lived plumes (lasting greater than ~ 80 Myr), and the mean plume lifespan was between 66 Myr ($Ra = 1 \cdot 10^7$) and 13.6 Myr ($Ra = 2 \cdot 10^8$).

The differential rate of motion between plumes at mid-mantle depth and the mantle increased with increasing Rayleigh number. We found that individual plumes can drift on average from 0.0617 - $0.223^\circ/\text{Myr}$ between $Ra = 1 \cdot 10^7$ and $Ra = 2 \cdot 10^8$. The net migration rate of plumes varied from 0.0162 - $0.0534^\circ/\text{Myr}$. The net motion of plumes is attenuated because symmetries between plumes can result in net zero move-

ment in the global convection. Comparing the lateral migration rates of plumes to the horizontal average velocity at mid-mantle and surface, there was a similar ratio for cases 3-5. The lateral velocity ratio (LVR) between plumes and the mid-mantle for these cases was ~ 0.35 , while between plumes and the surface was ~ 0.15 . This suggests that with increasing Rayleigh number, and therefore increasing mantle flow, there is a constant ratio drift of plumes relative to the mean mantle. We compared goodness-of-fit lines for the scaling of mean plume migration rate to Rayleigh number. The linear fit produced $R^2 = 0.9949$, and the power law $R^2 = 0.9323$. However, we suggest that there may be different regimes classifying the dependence of plume migration rates on Rayleigh number, perhaps dependent on the mode of convection. For example, the differences in long-wavelength structures between cases 7 and cases 3-5 might point to different plume- Ra scalings.

Zhong et al. (2000) argue that plate velocity boundary conditions control the morphology and scale of thermal convection in spherical shells. They produced models of thermal convection similar to those inferred from seismic tomography studies. In future we will incorporate plate motions into our models. We will also investigate the influences of thermochemical convection on plume fixity and presence, similar to *McNamara and Zhong* (2004), but in a 3-D spherical shell. We prescribed isothermal boundary conditions in our models, but radiogenic heating within the mantle is thought to contribute greatly to the thermal evolution of the mantle.

The majority of hot material supplied to hotspots at the surface is concentrated in the upper portion of the plume conduit. Hence, hotspots can persist even when the plume conduit has sheared due to differential advection in the mantle. Our studies quantified plume motion at mid-mantle depth, but an account of the evolution of the radial and lateral plume conduit geometry, as well as thermal flux, remains.

References

- Anderson, D.L. and King, S.D., 2014, Driving the Earth Machine?, *Science*, v. 346, 1184-1185.
- Becker, T.W., 2008, Azimuthal seismic anisotropy constrains net rotation of the lithosphere: *Geophysical Research Letters*, v. 35, p. 1-5, doi: 10.1029/2007GL032928.
- Conrad, C.P. and Behn, M.D., 2010, Constraints on lithosphere net rotation and asthenospheric viscosity from global mantle flow models and seismic anisotropy: *Geochemistry, Geophysics, Geosystems*, v. 11, p. 1-19, Q05W05, doi: 10.1029/2009GC002970.
- Courtilot, V., Davaille, A., Besse, J. and Stock, J., 2003, Three distinct types of hotspots in the Earth's mantle: *Earth and Planetary Science Letters*, v. 205, p. 295-308.
- Dobrovinić, P.V., Steinberger, B. and Torsvik, T.H., 2012, Absolute plate motions in a reference frame defined by moving hot spots in the Pacific, Atlantic, and Indian oceans: *Journal of Geophysical Research*, v. 117, p. 1-30, doi:10.1029/2011JB009072
- Duncan, R.A., 1981, Hotspots in the Southern Oceans – an absolute frame of reference for motion on the Gondwana continents: *Tectonophysics*, v. 74, p. 29-42, doi:10.1016/0040-1951(81)90126-8.
- Gripp, A.E. and Gordon, R.G., 2002, Young tracks of hotspots and current plate velocities: *Geophysical Journal International*, v. 150, p. 321-361.
- Jellinek, A.M and Manga, M., 2004, Links between long-lived hot spots, mantle plumes, and plate tectonics: *Reviews of Geophysics*, v. 42, p. 1-35.
- McNamara, A. and Zhong, S., 2004, The influence of thermochemical convection on the fixity of mantle plumes: *Earth and Planetary Science Letters*, v. 222, p. 485-500.
- Molnar, P. and Stock, J., 1987, Relative motions of hotspots in the Pacific, Atlantic and Indian Oceans since late Cretaceous time, *Nature*, v. 327, p. 587-591.
- Morgan, J., 1971, Convection plumes in the lower mantle: *Nature*, v. 230, 42-43.
- Morgan, J., 1981, Hotspot tracks and the opening of the Atlantic and Indian oceans: *Processes of Planetary Rifting*, v. 457, p. 1-4.
- O'Neill, C., Müller, R.D. and B. Steinberger (2005), On the uncertainties in hot spot reconstructions and the significance of moving hot spot reference frames: *Geochemistry, Geophysics, Geosystems*, v. 6, p. 1-35, Q04003, doi:10.1029/2004GC000784.
- Rudolph, M.L. and Zhong, S.J., 2014, History and dynamics of net rotation of the mantle and lithosphere: *Geochemistry, Geophysics, Geosystems*, v. 15, p. 1-13, doi:10.1002/2014GC005457.
- Seton, M., et al., 2012, Global continental and ocean basin reconstructions since 200 Ma: *Earth-Science Reviews*, v. 113, p. 212-270, doi:10.1016/j.earscirev.2012.03.002.
- Sleep, N.H., 2006, Mantle plumes from top to bottom: *Earth-Science Reviews*, v. 77, p. 231-271.
- Steinberger, B. and O'Connell, R.J., 1998, Advection of plumes in mantle flow: implications for hotspot motion, mantle viscosity and plume distribution: *Geophysics Journal International*, v. 132, 412-434.
- Whitehead, J.R. and Luther, D.J., 1975, Dynamics of laboratory diapir and plume models: *Journal of Geophysical Research*, v. 80, 705-717.
- Wolfe, C.J., Bjarnason, I.Th., VanDecar, J.C. and Solomon, S.C., 1997, Seismic structure of the Iceland mantle plume: *Nature*, v. 385, p. 245-247.
- Zhong, S., Zuber, M.T., Moresi, L. and Gurnis, M., 2000, Role of temperature-dependent viscosity and surface plates in spherical shell models of mantle convection: *Journal of Geophysical Research*, v. 105, p. 11063-11082.
- Zhong, S.J., 2001, Role of ocean-continent contrast and continental keels on plate motion, net rotation of lithosphere and the geoid, *Journal of Geophysical Research*, v. 106, p. 703-712, doi:10.1029/2000JB900364.
- Zhong, S., McNamara, A., Tan, E., Moresi, L. and Gurnis, M., 2008, A benchmark study on mantle convection in a 3-D spherical shell using CitcomS: *Geochemistry, Geophysics, Geosystems*, v. 9, p. 1-32.
- Schubert, G., Turcotte, D.L. and Olson, P., 2001, *Mantle convection in the Earth and planets*, Cambridge University Press, Cambridge, 940 pp.